Article

Neuron

Regional Blood Flow in the Normal and Ischemic Brain Is Controlled by Arteriolar Smooth Muscle Cell Contractility and Not by Capillary Pericytes

Highlights

- Pericytes are morphologically and functionally distinct from precapillary SMCs
- Capillary pericytes lack smooth muscle actin and are not contractile in vivo
- Neurovascular coupling is mediated by arteriolar smooth muscle contractility
- Ischemia causes transient SMC constrictions that lead to capillary thrombosis

Authors

Robert A. Hill, Lei Tong, Peng Yuan, Sasidhar Murikinati, Shobhana Gupta, Jaime Grutzendler

Correspondence

jaime.grutzendler@yale.edu

In Brief

The extent to which arteriolar smooth muscle cell or capillary pericyte contractility regulates regional cerebral blood flow is debated. Hill et al. use optogenetic, whisker stimulation, spreading depolarization, and transient cerebral ischemia to demonstrate that capillary pericytes are not contractile in vivo and that arteriolar smooth muscle cells mediate physiological and pathological vasomotion.

Hill et al., 2015, Neuron *87*, 95–110
July 1, 2015
http://dx.doi.org/10.1016/j.neuron.2015.06.001

CellPress

Neuron
Article

Regional Blood Flow in the Normal and Ischemic Brain Is Controlled by Arteriolar Smooth Muscle Cell Contractility and Not by Capillary Pericytes

Robert A. Hill,[1,2,3] Lei Tong,[1,2,3] Peng Yuan,[1,2,3] Sasidhar Murikinati,[1,2] Shobhana Gupta,[1,2] and Jaime Grutzendler[1,2,*]
[1]Department of Neurology
[2]Department of Neurobiology
Yale School of Medicine, New Haven, CT 06510, USA
[3]Co-first author
*Correspondence: jaime.grutzendler@yale.edu
http://dx.doi.org/10.1016/j.neuron.2015.06.001

SUMMARY

The precise regulation of cerebral blood flow is critical for normal brain function, and its disruption underlies many neuropathologies. The extent to which smooth muscle-covered arterioles or pericyte-covered capillaries control vasomotion during neurovascular coupling remains controversial. We found that capillary pericytes in mice and humans do not express smooth muscle actin and are morphologically and functionally distinct from adjacent precapillary smooth muscle cells (SMCs). Using optical imaging we investigated blood flow regulation at various sites on the vascular tree in living mice. Optogenetic, whisker stimulation, or cortical spreading depolarization caused microvascular diameter or flow changes in SMC but not pericyte-covered microvessels. During early stages of brain ischemia, transient SMC but not pericyte constrictions were a major cause of hypoperfusion leading to thrombosis and distal microvascular occlusions. Thus, capillary pericytes are not contractile, and regulation of cerebral blood flow in physiological and pathological conditions is mediated by arteriolar SMCs.

INTRODUCTION

Cerebral function consumes a large amount of energy; however, the precise locations and extent of neural activity within regions of the brain are constantly fluctuating. Consequently, the brain has evolved a specialized system to ensure coupling between energy demand and supply through precise spatial and temporal modulation of cerebral blood flow (CBF) (Hamel, 2006; Iadecola, 2004; Raichle and Mintun, 2006; Roy and Sherrington, 1890). While the mechanisms controlling neurovascular coupling are not well understood, previous work demonstrates the involvement of complex interactions between neurons, glia, and vascular cells (Haydon and Carmignoto, 2006; Iadecola and Nedergaard, 2007; Kety and Schmidt, 1948; Roy and Sherrington, 1890). Neural activation induces transient local microvascular dilations, leading to increased blood flow and tissue oxygenation, a phenomenon that forms the basis for functional magnetic resonance imaging (fMRI) (Logothetis et al., 2001; Ogawa et al., 1990). The modulation of vessel diameter, vascular resistance, and blood flow is controlled by cells within the microvascular wall (mural cells), which have contractile properties. A precise understanding of the function of these cells in vivo is important not only for investigating the source of the signals obtained with fMRI blood-oxygen-level-dependent (BOLD) techniques (Attwell and Iadecola, 2002; Logothetis and Wandell, 2004; Raichle and Mintun, 2006) but also for elucidating the pathophysiology of many diseases involving the brain microvasculature (Iadecola and Nedergaard, 2007; Puro, 2007; Winkler et al., 2014).

Mural cells on the cerebral vascular tree include arteriolar and venular smooth muscle cells (SMCs) and capillary pericytes (Rouget, 1874). These cells are thought to play important roles in microvascular development, angiogenesis (Armulik et al., 2010; Daneman et al., 2010), and maintenance of the blood brain barrier (Bell et al., 2010), and are implicated in a variety of neuropathological conditions (Bell et al., 2010; Hall et al., 2014; Sagare et al., 2013; Yemisci et al., 2009). It is well known that microvascular smooth muscle regulates vessel diameter and blood flow (Brian et al., 1998; Devor et al., 2007; Fernández-Klett et al., 2010; Kornfield and Newman, 2014; Vanzetta et al., 2005). However, within brain microregions, the precise location where neural activity-induced vasomotion is modulated is less clear. Specifically, which segments of the vascular tree, especially at the transition between arterioles and terminal capillaries, are the primary sites of CBF regulation remains a topic of debate (Armulik et al., 2011; Hamilton et al., 2010; Iadecola and Nedergaard, 2007; Itoh and Suzuki, 2012; Krueger and Bechmann, 2010; Winkler et al., 2011).

Recent studies have suggested capillaries to be major sites for active CBF regulation (Chaigneau et al., 2003; Hall et al., 2014; Peppiatt et al., 2006). In fact, it was estimated that up to 84% of blood flow modulation may take place at the terminal capillary level, where pericytes are the predominant mural cell, suggesting that these cells have prominent contractile properties (Hall et al., 2014). However, separate studies in the cortex and retina suggest that while pericyte contractility does occur, the direct

role of capillaries in flow control may not be very significant (Fernández-Klett et al., 2010; Kornfield and Newman, 2014). In addition to physiological control of microvascular flow, in cerebral ischemia, constriction of capillary pericytes that persists after their death has been proposed to prevent tissue reperfusion, leading to the "no-reflow" phenomenon (Hall et al., 2014; O'Farrell and Attwell, 2014; Yemisci et al., 2009). However, the difficulty in distinguishing the various mural cell types in vivo, especially at the transition between arterioles and capillaries, and the variability in experimental methodologies have brought the concept of physiological and pathological capillary pericyte contractility into question (Vates et al., 2010). Resolution of these discrepancies is of great importance not only because of its implications for modeling physiological microregional blood flow and brain oxygenation, but also for understanding the role of the microvasculature and mural cells in neuropathological conditions.

We utilized a combination of genetically encoded microvascular mural cell labeling, high-resolution imaging of vasomotor activity, functional calcium imaging, and optogenetic cell activation to precisely characterize the structural and functional properties of cerebral vascular mural cells in vivo. We demonstrate that capillaries are incapable of active vasomotor responses to a variety of stimuli such as direct pericyte optogenetic stimulation, physiological neural activation, and spreading depolarization. Pericytes in brain capillaries completely lack expression of smooth muscle actin (SMA), consistent with our finding that only microvessels enveloped by mural cells with a circumferential band-like morphology, typical of smooth muscle, display active vasomotor responses. Furthermore, we find that the diameter and branch order of precapillaries with circumferential smooth muscle is frequently indistinguishable from that of pericyte-covered capillaries. Thus, ambiguous distinction between these cell types could partly explain contradicting reports about capillary pericyte contractility. Finally, we demonstrate that during brain ischemia, SMC but not pericyte constriction leads to vessel occlusion due to secondary thrombus formation within distal microvessels. Our study provides functional and structural in vivo evidence defining the cellular components of the microvascular contractile apparatus, with important implications for future studies of the normal and pathological regulation of CBF.

RESULTS

Morphologically Distinct Mural Cells along the Brain Microvascular Tree

In order to perform a comprehensive study of the vasomotor properties of mural cells, we first set out to determine their precise distributions and morphological features at various locations within the vascular tree in the mouse cerebral cortex. A detailed morphological analysis was necessary in order to accurately define the various mural cells that could potentially control CBF, as inconsistencies in cell definition and identification likely contribute to contradicting reports in the literature. We first imaged mice that expressed membrane-bound GFP (mGFP) specifically in cells with constitutive or inducible Cre recombinase driven by the NG2 promoter (*NG2cre:mT/mG* and *NG2creER:mT/mG*). *NG2cre* mice have Cre expression specifically in SMCs, pericytes, NG2 cells, and oligodendrocytes, each of which can be clearly distinguished by their morphology and close association with vessels, as described previously (Hill et al., 2014; Zhu et al., 2008). In constitutive *NG2cre* mice, Cre recombination efficiency was sufficient to observe near-complete mGFP labeling of NG2-expressing mural cells, while single isolated cells could be visualized in inducible *NG2creER* mice after a single injection of tamoxifen. This approach revealed cells with distinct morphologies at each level of the vascular tree (Figure 1 and see Figure S1 available online).

Cells with classical smooth muscle morphology, forming narrow circumferential bands that surround the entire vessel, were found on pial and penetrating arterioles with diameters ranging from 15 to 40 μm (Figures 1A and S1). On more distal vessels, 3–15 μm in diameter, we also observed similar band-like cells with variable lengths, all of which enveloped the entire vessel circumference (Figures 1B–1G and S1). Based on their circumferential band-like morphology, we classified these two mural cell populations as arteriole and precapillary SMCs, respectively. Within the subset of smaller microvessels, with diameters ranging from 3 to 9 μm, we also observed morphologically distinct cells with processes that extended longitudinally for hundreds of microns along multiple capillary branchpoints (Figures 1B–1H and S1). In addition to their long processes, these cells also had short and thin processes that projected orthogonally across the vessel but rarely spanned its entire circumference (Figure S1). We classified this type of cell as capillary pericytes, due to their unique morphology and location. Immediately adjacent cells in postcapillary venules displayed a band-like circumferential phenotype similar to arteriolar smooth muscle, but spanned larger distances and had a highly fenestrated patchwork-like appearance (Figures 1A, 1B, and 1G).

To further distinguish the various mural cell types, we crossed *NG2cre* mice with the brainbow-like Cre dependent *confetti* reporter (*NG2cre:confetti*). Consistent with mT/mG reporter mice, we could precisely identify morphologically distinct single cells (due to differential fluorescent protein labeling) with either SMC or pericyte morphology, further delineating the single cell territories and discrete morphologies of each cell type (Figure S2).

Spontaneous Vasomotion and Mural Cell Calcium Fluctuations in Awake Mice

We then set out to determine the contractile properties of vessels at various levels of the vascular tree. We used in vivo two-photon imaging to measure spontaneous single-vessel diameter changes in the somatosensory cortex of awake head-fixed *NG2cre:ZEG* mice injected with an intravascular dye to visualize all vessels. In vivo time-lapse imaging in these mice revealed that 10–50 μm diameter arterioles with a layer of cells with SMC morphology spontaneously dilated and contracted at relatively high frequencies, while venules rarely displayed significant diameter changes. We focused our analysis on vessels smaller than 10 μm in diameter, as this is where we observed the transition from precapillary SMCs to capillary pericytes (Figures 1 and 2A–2D). Consistent with the heterogeneous mural cell morphology that we observed, these vessels displayed highly variable spontaneous vasomotion that did not correlate well

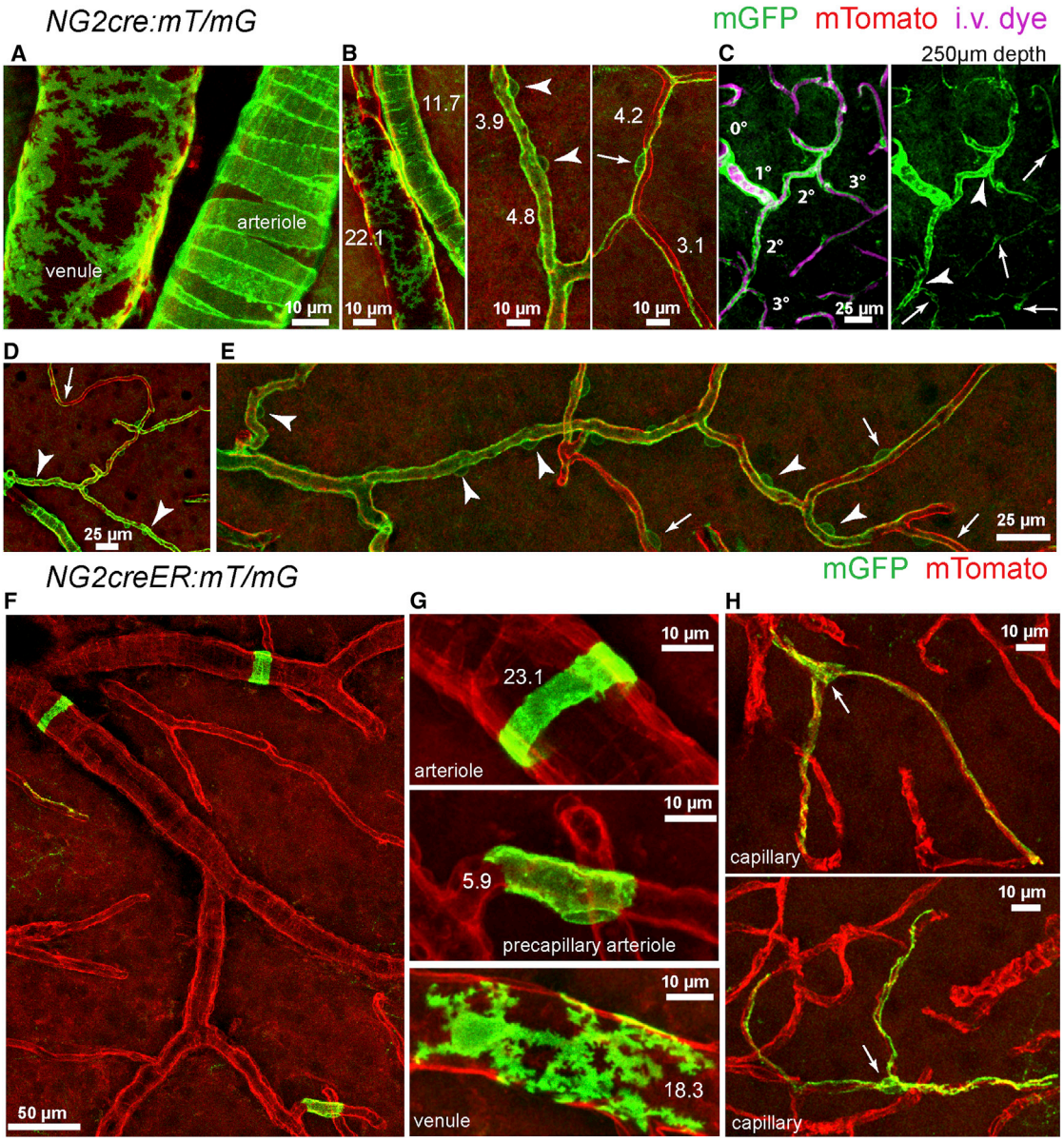

Figure 1. Distinct Morphology of Mural Cells along the Cortical Vascular Tree

(A) In vivo image captured from the cortex of an *NG2cre:mT/mG* transgenic mouse showing mGFP (green)-expressing smooth muscle cells on arterioles and venules with mTomato (red) expression in all membranes.

(B) In vivo images showing detailed morphology of mGFP labeled cells on pre- and postcapillary vessels (left), precapillary arterioles covered by single smooth muscle cells (middle, arrowheads), and capillaries covered by a single pericyte (right, arrow); numbers indicate vessel diameter.

(C) In vivo two-photon image showing mGFP expression on a penetrating arteriole and several branches (branch order indicated) demonstrating the transition from smooth muscle cell morphology (arrowheads) to capillary pericytes (arrows). Vessels are labeled via intravascular dye.

(D and E) Images showing transitions from mGFP-labeled smooth muscle cell morphology (arrowheads) to capillary pericytes (arrows).

(F) Image captured from the cortex of an *NG2creER:mT/mG* transgenic mouse showing isolated mGFP-labeled cells after a single injection of tamoxifen.

(G) Single-cell circumferential morphology of smooth muscle cells on arterioles (top), precapillary arterioles (middle), and postcapillary venules (bottom); numbers indicate vessel diameter.

(H) Single-cell morphology of capillary pericytes extending longitudinally over hundreds of microns (arrows).

See also Figures S1 and S2.

with their respective diameters (Figure 2A–2D; Movie S1). To accurately describe this contractile behavior, we quantified the area under the curve of the percent changes in vessel diameter (Figures 2C, 2F, and 2G), a measure that accounts for amplitude, frequency, and duration of diameter changes, and which we termed vasomotion index (see Experimental Procedures). This

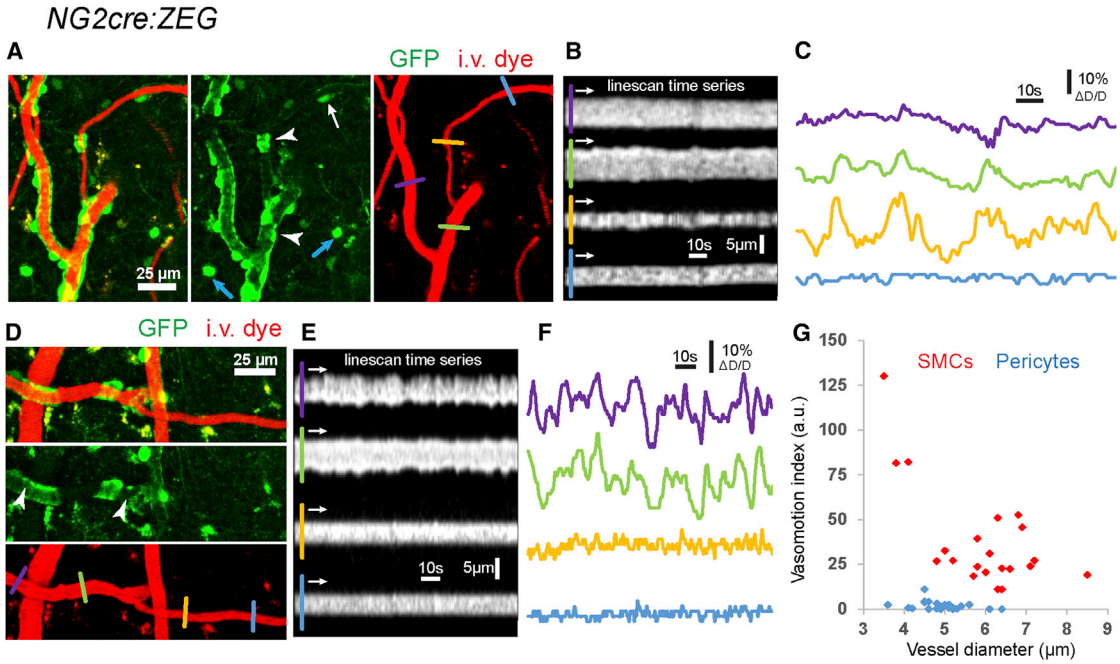

Figure 2. Awake Imaging of Spontaneous Vasomotion along the Cortical Vascular Tree

(A) In vivo images captured from the cortex of awake head-fixed *NG2cre:ZEG* transgenic mice showing GFP (green) labeled smooth muscle (arrowheads), pericytes (white arrows), and NG2 cells (blue arrows), while vessels are labeled via intravascular dye (red).

(B) Line-scan time series showing spontaneous diameter changes of the vessels shown in (A).

(C) Diameter changes of four vessel segments with (magenta, green, orange) or without (blue) smooth muscle cells shown in (A) and (B).

(D) Smooth muscle cells on a precapillary arteriole (arrowheads).

(E) Line-scan time series showing spontaneous diameter changes of the vessels shown in (D).

(F) Diameter changes of the four vessel segments with (magenta and green) or without (orange and blue) smooth muscle cells shown in (D) and (E).

(G) The relationship between vessel diameter and a vasomotion index defined as the area under the curve for percent spontaneous changes in vessel diameter with a ±5% cutoff threshold, n = 47 vessel segments from 4 mice.

See also Movie S1.

quantification revealed that the heterogeneous spontaneous diameter changes were clearly correlated to the type of mural cell covering these vessels (Figure 2G) (vasomotion indices: precapillary SMC-covered vessels 38.2 ± 6.3; capillary pericyte-covered vessels 1.8 ± 0.5, $p < 0.001$ unpaired t test).

To further characterize and correlate a functional intracellular signal in single mural cells with changes in vessel diameter, we generated mice with a Cre-dependent genetically encoded calcium indicator (GCaMP3) expressed specifically in NG2-positive mural cells (and some neurons, see below) (*NG2cre:GCaMP3*). Detailed analysis of changes in GCaMP3 fluorescence intensity showed SMC calcium transients preceding, coinciding with, or following vasomotion, with a significant anticorrelation between increases in SMC calcium and vessel dilation (Figures 3A, 3B, and 3F; Movie S1) (correlation, $r = -0.49 \pm 0.21$ SD, $n = 24$ vessel segments from 3 mice, significant differences from 0 correlation determined by a 99% confidence interval).While transient robust changes in GCaMP3 fluorescence were also detected in pericytes, no changes in vessel diameter were detected (Figures 3C and 3D; Movie S3), and thus there was no correlation between pericyte calcium fluctuations and changes in vessel diameter (Figures 3E and 3F) (correlation, $r = 0.02 \pm 0.07$ SD, $n = 12$ pericytes from 3 mice).

These morphological and functional data suggested that the presence or absence of the different mural cell types determined whether active vasomotion occurred in individual microvessels. To directly test this hypothesis, we next looked for the presence of contractile proteins to correlate molecular and cellular identity with in vivo function.

Expression of Smooth Muscle Actin in Arterioles but Not Capillaries in Mice and Humans

To understand the reasons behind the heterogeneous contractility in smaller vessels, we performed in vivo imaging of double transgenic mice expressing the fluorescent protein mCherry driven by the SMA promoter and endothelial GFP driven by the Tie2 promoter (*SMA-mCherry:Tie2-GFP*). In these mice, all vessels were labeled with GFP, and arterioles were enveloped with a bright layer of *SMA-mCherry*-labeled mural cells (Figures 4A and 4B). Artery specificity of mCherry was determined by the directionality of the blood flow and confirmed by labeling with intravenously injected Alexa Fluor 633 hydrazide (Figure S4), which binds to the elastin layer in arterioles (Shen et al., 2012). In addition to detecting bright *SMA-mCherry* on large penetrating arteries and arterioles, we often observed mCherry expression on smaller vessels with diameters less than 10 µm (Figures

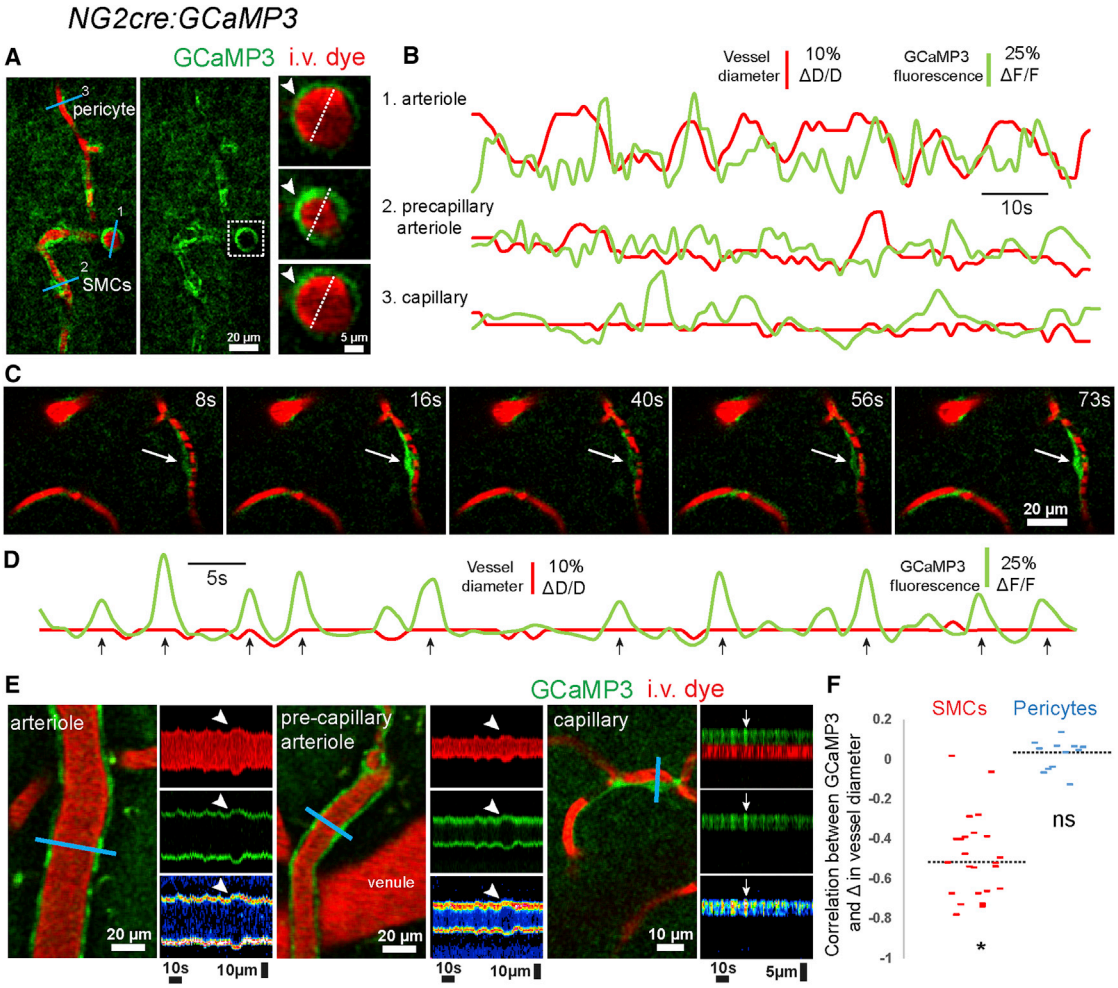

Figure 3. Correlation between Vasomotion and Calcium Transients in Mural Cells In Vivo

(A) In vivo image from the cortex of an *NG2cre:GCaMP3* transgenic mouse showing a penetrating arteriole and the transition from SMC-covered (1 and 2) to pericyte-covered (3) vessels. Time-lapse sequences show the change in vessel diameter (dotted line) and corresponding changes in GCaMP3 fluorescence (arrowheads).

(B) Traces of spontaneous changes in vessel diameter (red) overlayed with corresponding changes in GCaMP3 calcium fluorescence (green) in SMC-covered arterioles and pericyte-covered capillaries.

(C) Time-lapse sequence showing spontaneous GCaMP3 calcium changes in a single pericyte cell body (arrow) and processes.

(D) Traces of changes in vessel diameter (red) overlayed with changes in pericyte GCaMP3 calcium signals (green). Arrows indicate changes in pericyte calcium with no changes in capillary diameter.

(E) Example images and line-scan time series at each level of the vascular tree. Changes in vessel diameter occurred only on SMC-covered vessels which corresponded to decreases in SMC GCaMP3 calcium signals (arrowheads). In contrast, peaks in pericyte calcium (arrow) correlated with no change in capillary diameter.

(F) Quantification of the correlation between GCaMP3 calcium signals and changes in vessel diameter in SMCs (red) r = −0.49 ± 0.21 SD, and pericytes (blue) r = 0.02 ± 0.07 SD, n = 24 SMC-covered vessels and 12 pericyte-covered vessels from 3 mice; asterisk indicates significant differences from 0 correlation determined by a 99% confidence interval.

See also Movie S2 and Movie S3.

4C–4G). Quantification revealed that the last *SMA-mCherry*-expressing cells at the transition between arterioles and capillaries were found at both branchpoints and in the middle of single vessels with diameters ranging from 3.3 to 8.5 µm (Average of 5.4 ± 1.3 µm) and branch orders ranging from first to fourth (0 being a penetrating arteriole) (n = 45 vascular tress from 4 mice) (Figures 4C–4J). Unexpectedly, at the location of these terminal *SMA-mCherry*-expressing cells, we frequently observed that the vessel diameter was smaller compared to the downstream capillary (Figure 4G), strongly suggesting that mural cells in capillaries are not capable of providing a baseline contractile tone like distal SMCs.

To verify that the observed lack of SMA expression in capillaries was not due to incomplete mosaic expression in our *SMA-mCherry* transgenic mice, we confirmed our observations with immunohistochemistry for SMA (Figure 4K) as well as in a

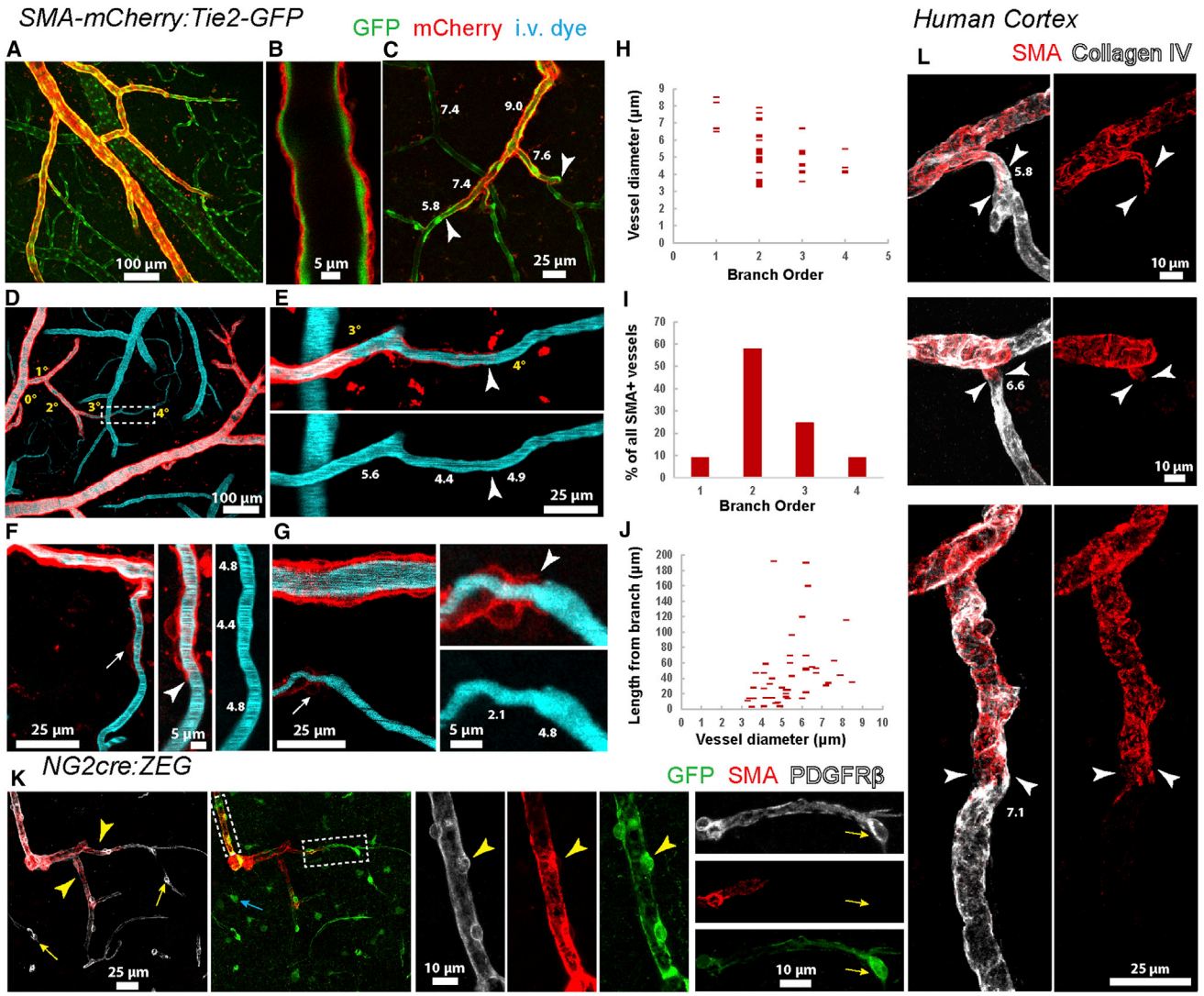

Figure 4. Smooth Muscle Actin Is Expressed by Arteriole but Not Capillary Mural Cells in Mouse and Human Neocortex

(A) In vivo image captured from the cortex of a smooth muscle actin *(SMA)-mCherry:Tie2-GFP* transgenic mouse showing GFP (green) labeling in all vessels and bright mCherry (red) expression in arterioles and precapillary vessels.

(B) A single GFP-labeled arteriole enveloped by a layer of SMA-labeled mCherry.

(C) Branching of a precapillary vessel showing the termination of *SMA-mCherry*-expressing cells (arrowheads) with vessel diameter indicated adjacent to single vessels.

(D) *SMA-mCherry* expression in surface and penetrating arterioles with vessels labeled via intravascular dye (cyan). Vessel branch orders indicated in yellow.

(E) High-magnification image of the vessel outlined in (D) showing the termination of the last *SMA-mCherry*-expressing cell (arrowheads) on a fourth branch order vessel; numbers in lower panel indicate vessel diameter.

(F and G) *SMA-mCherry* expression on precapillary vessels at different vascular tree levels. The last *SMA-mCherry*-expressing cells (panels on the right indicate zoomed regions of terminal SMA+ cells shown on the left) are indicated with cell bodies (arrows) and terminal processes (arrowheads); numbers indicate vessel diameter.

(H) Correlation of vessel branch order with that of the distribution of vessel diameters where the last *SMA-mCherry*-expressing smooth muscle cell is located.

(I) The percentage breakdown for the branch order on which terminal SMA+ cells are located.

(J) Correlation of vessel diameter with the distance from a vessel branch point where the last *SMA-mCherry*-expressing smooth muscle cell is located.

(K) Immnohistochemical staining of *NG2cre:ZEG* mouse necortex with antibodies for SMA (red) and PDGFRβ (white) showing that SMA locates only at SMCs on arterioles and precapillary arterioles (yellow arrowheads), while PDGFRβ is expressed by both arteriolar SMCs and capillary pericytes (yellow arrows). GFP-labeled cells in the parenchyma (blue arrows) are oligodendrocyte lineage cells.

(L) Immunohistochemical staining of human neocortex with antibodies for collagen IV (white) to label blood vessels and SMA (red) showing the transition from SMA-covered precapillary arterioles to SMA-lacking capillaries (arrowheads); numbers indicate vessel diameter.

See also Figure S3.

separate transgenic line with mGFP expressed specifically in SMA+ cells (*SMAcreER:mT/mG*) (Figure S3). SMA antibody staining showed identical expression to *SMA-mCherry* mice and was not found in pericytes (Figures 4K and S4). In addition to NG2 and SMA, expression of the β receptor for platelet derived growth factor (PDGFRβ) is routinely used to identify pericytes. Importantly however, we found expression of PDGFRβ on both SMA+ SMCs and SMA− pericytes (Figures 4K and S4).

In addition to seeing *SMA-mCherry*-labeled cells on arteries and precapillary arterioles, due to bright fluorescence in these mice, we also observed weak mCherry expression on large venules (>50 μm), but not on smaller postcapillary vessels (Figure S3), suggesting that large venules have some limited contractile potential. Importantly, the SMA expression in arterioles and its absence from terminal capillaries was not unique to mice, as we also observed it in human neocortex (Figure 4J). Quantification of postmortem human tissues stained with antibodies against SMA revealed that 8.5% ± 0.3% of the total length of human intraparenchymal cerebral vessels (n = 3 human samples) was enveloped with SMA-expressing mural cells. Similar to mice, the last SMA-expressing cells at the transition between arterioles and capillaries were found at both branchpoints and in the middle of single vessels, ranging from 4.63 to 15.5 μm in diameter (average diameter 9.1 ± 0.4 μm, n = 41 vascular trees from three human samples).

These data provide strong evidence that, regardless of vessel diameter or branch order, SMA is expressed in mural cells with circumferential SMC morphology but is absent from pericytes. This provides a likely explanation for the heterogeneity in spontaneous vasomotion that we observed at the precapillary versus capillary levels (Figure 2).

Optogenetic-Induced Vasomotion Only Occurs in Smooth Muscle-Covered Vessels

To directly assess the contractile properties of individual cells at various levels of the vascular tree, we generated double transgenic mice which express a light gated proton channel (channelrhodopsin 2, ChR2) fused to yellow fluorescent protein (YFP) specifically in NG2-expressing cells (*NG2cre:ChR2-YFP*) and crossed them with *SMA-mCherry* mice to generate *NG2cre:ChR2-YFP:SMA-mCherry* triple transgenic mice. These mice express ChR2-YFP in cortical pericytes, SMCs, oligodendrocyte lineage cells, and a small number of cortical astrocytes as well as mCherry in all SMCs (Figure 5A). The presence of voltage-gated calcium channels in both SMCs and pericytes (Figure S5) (Borysova et al., 2013; Sakagami et al., 1999), assured that ChR2 stimulation would cause depolarization of both cell types.

Using these mice, we implemented a confocal laser line-scan technique to optimally activate ChR2 and cause targeted mural cell stimulation while simultaneously imaging vessel diameter (see Experimental Procedures). In arterioles larger than 10 μm in diameter, which were covered by SMA-expressing SMCs, light activation caused significant vessel constrictions (−19.41 ± 1.90% change in diameter, n = 58 vessels from 8 mice) (Figures 5B–5E). Similarly, light activation on vessels less than 10 μm in diameter but still covered by SMA-expressing precapillary SMCs, resulted in significant vessel constrictions (Figures 5B–5E) (−11.79 ± 2.06% constriction, n = 18 vessels from 8 mice). In contrast, vessels less than 10 μm in diameter covered by pericytes but not SMA-expressing SMCs showed no constriction after identical light activation of ChR2 (Figures 5B–5E) (0.08 ± 0.18% change in diameter, 39 vessels from 8 mice). To exclude possible artifacts by non-mural-cell ChR2 stimulation in constitutive *NG2cre:ChR2-YFP* mice, we used low-dose tamoxifen induction in *NG2creER:ChR2-YFP*, where we were able to label cells very sparsely to isolate individual SMCs and pericytes, thus removing any concern about nearby expressing cells. ChR2 stimulation of isolated cells demonstrated the same results, with SMC constriction and lack of pericyte contractility (Figure S5).

Given that small and potentially difficult to detect changes in vessel diameter can induce substantial changes in blood flow proportional to the fourth power of radius changes (as per Poiseuille equation of fluid dynamics), we directly tested the impact of targeted ChR2 activation on blood-flow velocity. In order to avoid potential out of focal plane ChR2 activation by the confocal laser, which could prevent accurate local flow measurements due to proximal vessel constrictions, we used instead targeted two-photon stimulation of ChR2 within small regions of interest (ROIs) along single vessels. Consistent with the observed constrictions, ChR2 activation on vessels covered by SMCs significantly reduced blood flow velocity (Figures 5F–5I) (−44.62 ± 11.80% change, n = 10 vessels from 3 mice), while ChR2 activation on vessels that were not covered by SMCs did not significantly change blood flow (Figure 5H-I) (−2.22 ± 3.16% change, n = 30 vessels from 3 mice). These data strongly demonstrate that in the intact mouse neocortex, single-cell depolarization of SMCs, but not pericytes, results in robust modulation of vessel diameter and CBF.

Neural Activity-Induced Vasomotion Does Not Occur in Pericyte-Covered Capillaries

To determine which vessels respond to an increase in neuronal activity and thus regulate functional hyperemia, we imaged the vascular response to whisker stimulation in the awake mouse somatosensory cortex. To correlate neuronal activity with vascular changes, we again used the *NG2cre:GCaMP3* transgenic mice. Unexpectedly, we found that in these mice both mural cells and neurons are brightly labeled (Figure 6A), likely due to ectopic neuronal Cre expression (Nishiyama et al., 2014). The dual labeling with GCaMP3 in neurons and NG2-expressing cells was very useful because it allowed us to identify and image vessels with SMCs and pericytes (Figure 6B) while concurrently monitoring neuronal activity (Figures 6C and 6D).

We performed in vivo time-lapse imaging of vessel diameter and neuronal and mural cell calcium changes during and after sensory stimulation in the awake mouse. Whisker stimulation (30 s of 5 Hz, 100 ms air puffs) evoked robust neuronal calcium transients and significant vessel dilations (~10% change at peak dilation) in somatosensory cortex vessels covered with smooth muscle (Figures 6E–6G) (significance determined by a 99% confidence interval, vessel diameter range 6.2–21 μm, branch order 0–3, n = 57 vessels from 4 mice). This immediate active dilation was not observed in vessels that lacked a smooth muscle layer (Figures 6E–6G) (vessel diameter range 3.3–8.1 μm,

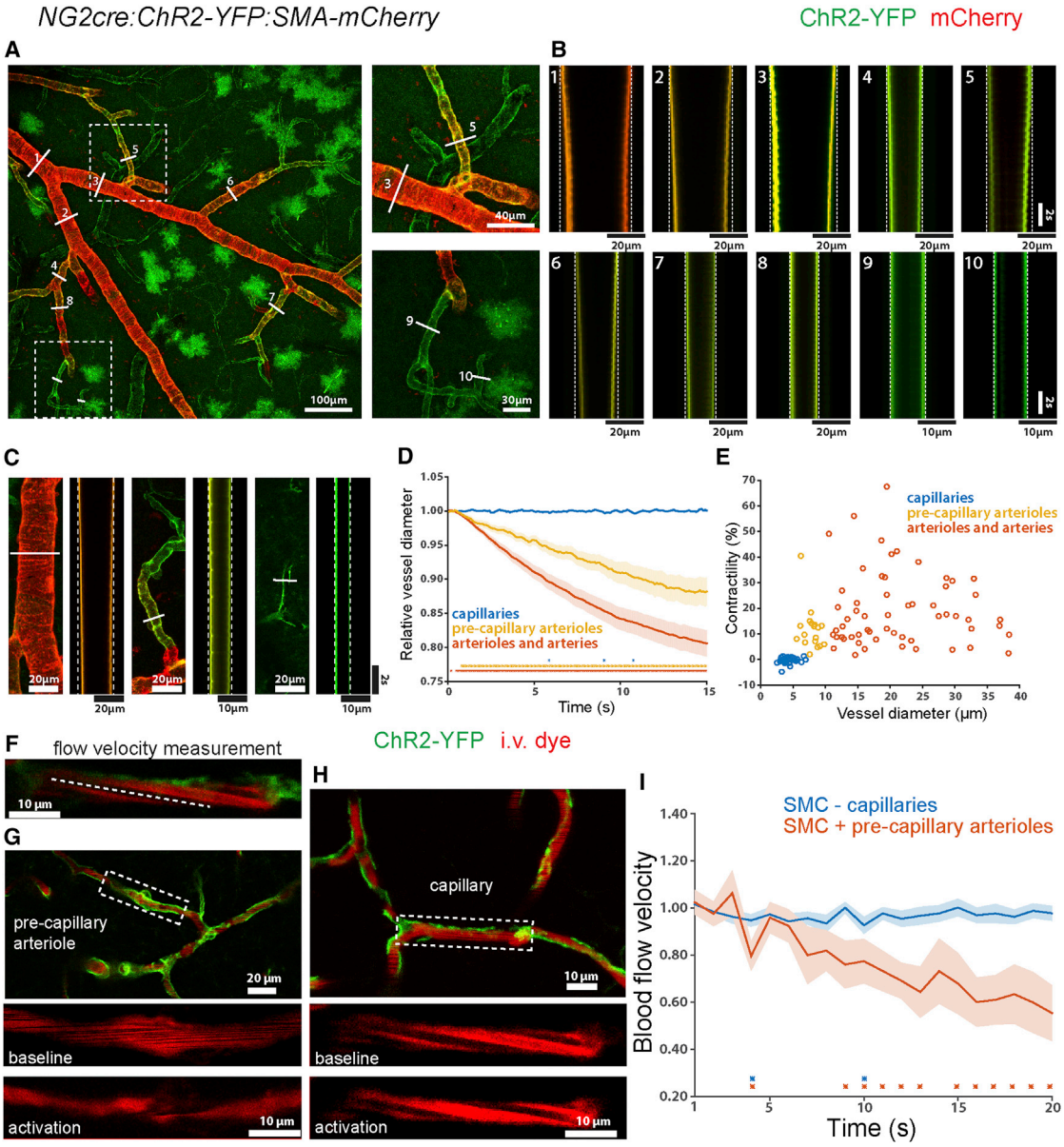

Figure 5. Single-Cell Optogenetic Activation Causes Vessel Constriction and Decreases Blood Flow in Smooth Muscle but Not Pericyte-Covered Microvessels

(A) In vivo images captured from the cortex of an *NG2cre:ChR2-YFP:SMA-mCherry* mouse showing SMA (red) expression on arterioles and precapillary arterioles and Chr2-YFP expression (green) on all vessels and a subpopulation of astrocytes.

(B) Line-scan time series images showing changes in vessel diameter after line-scan activation of ChR2 at various levels of the vascular tree with and without SMA (indicated by numbers with location identified with white lines [A]).

(C) Paired examples showing locations of ChR2 activation (white lines) on vessels with and without SMA, with corresponding line-scan time series images demonstrating that only SMA-covered vessels show vessel constriction.

(D) The average vessel diameter change in response to ChR2 activation (at time 0) on vessels with smooth muscle (arterioles, red line; precapillary arterioles, orange line) and without smooth muscle (capillaries, blue line). Traces show mean values ± SEM, n = 58 arterioles, 18 precapillary arterioles, and 39 capillaries from 8 mice. Asterisk indicates significance determined by a 99% confidence interval.

(E) The distribution of vessels that showed contractility in response to ChR2 activation in relation to vessel diameter.

(F) Method for determination of changes in blood flow velocity using the distortion of the image of a red blood cell as it moves (dotted line) during laser scanning (relative velocity field scanning).

(G) A decrease in vessel diameter and blood flow on a SMC-covered vessel after optogenetic activation.

(H) No change in blood flow velocity after optogenetic activation in a pericyte-covered vessel.

(I) Quantification of the average change in blood flow velocity during optogenetic activation in SMC+ precapillary arterioles (red line) and SMC− capillaries (blue line). Traces show mean values ± SEM, n = 10 precapillary arterioles and 30 capillaries from 3 mice. Asterisk indicates significance determined by a 99% confidence interval.

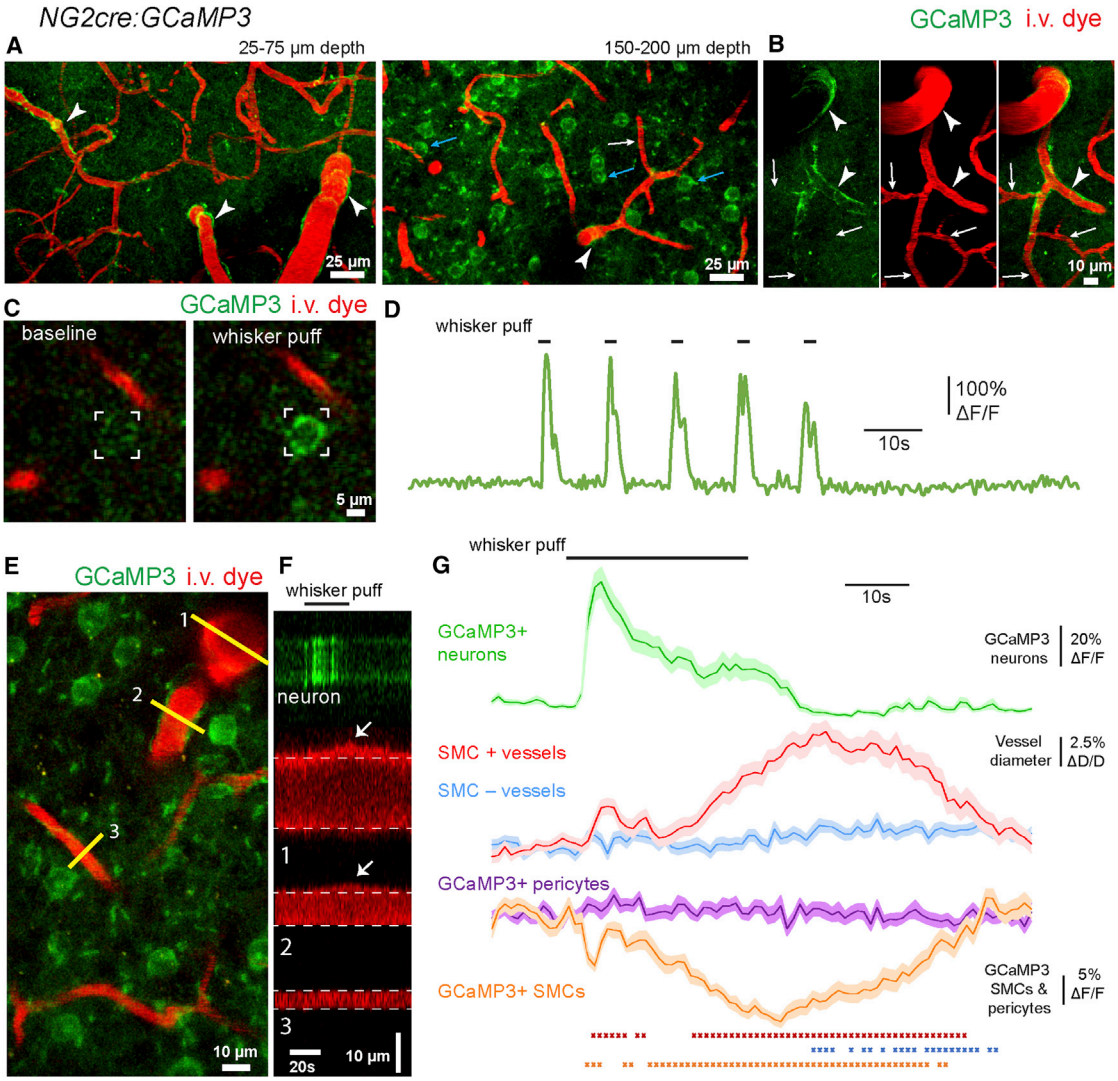

Figure 6. Smooth Muscle but Not Pericyte-Covered Microvessels Undergo Active Sensory-Evoked Vasodilatation in Awake Mice

(A and B) In vivo images captured from the somatosensory barrel cortex of awake head-fixed *NG2cre:GCaMP3* transgenic mice showing GCaMP3 (green) baseline fluorescence labeling of smooth muscle (arrowheads) and neurons (blue arrows) but very little in capillary pericytes (white arrows). Vessels are labeled via intravascular dye (red).

(C) A single neuronal calcium response (box) to a whisker puff detected by a fluorescence intensity increase of the GCaMP3 signal.

(D) Trace showing the percent change in neuronal GCaMP3 fluorescence to five repeated whisker puffs.

(E) Image showing examples of GCaMP3-positive and -negative vessels analyzed from time-lapse images during 30 s of whisker stimulation.

(F) Line-scan time series images showing the GCaMP3 neuronal response and whisker-evoked dilation (arrows) of the vessels shown in (E).

(G) Quantification of the neuronal and vascular responses to whisker stimulation (black bar) with the average neuronal GCaMP3 fluorescence signal (green), the average change in diameter of precapillary vessels with a smooth muscle layer (SMC+, red), capillaries lacking a smooth muscle layer (SMC−, blue), and GCaMP3 fluorescence signal in pericytes (magenta) and SMCs (orange). Traces show mean values ± SEM, n = 57 SMC+ vessel segments, 83 SMC− vessel segments from 4 mice for neuronal response and vessel diameter, and n = 24 SMCs and 12 pericytes from 3 mice for GCaMP3 traces. Asterisk indicates significance compared to baseline determined by a 99% confidence interval coded by color for corresponding cell type (SMC or pericyte) and signal (vessel diameter or GCaMP3).

branch order 1–4, n = 83 vessels from 4 mice). While, there was a slight (~1%) delayed dilation in vessels lacking smooth muscle, this occurred after peak dilation had occurred in vessels with SMCs, an effect that is most likely a passive result of upstream increases in blood flow (Figure 6G). Whisker stimulation also induced a robust decrease in calcium-dependent GCaMP3 fluorescence in SMCs which correlated temporally with changes in vessel diameter (Figure 6G) (significance determined by a 99% confidence interval, n = 19 vessel segments from 3 mice). In contrast, changes in calcium-dependent GCaMP3 fluorescence in pericytes were not correlated with whisker stimulation (Figure 6G) (n = 27 vessel segments from 3 mice). These data

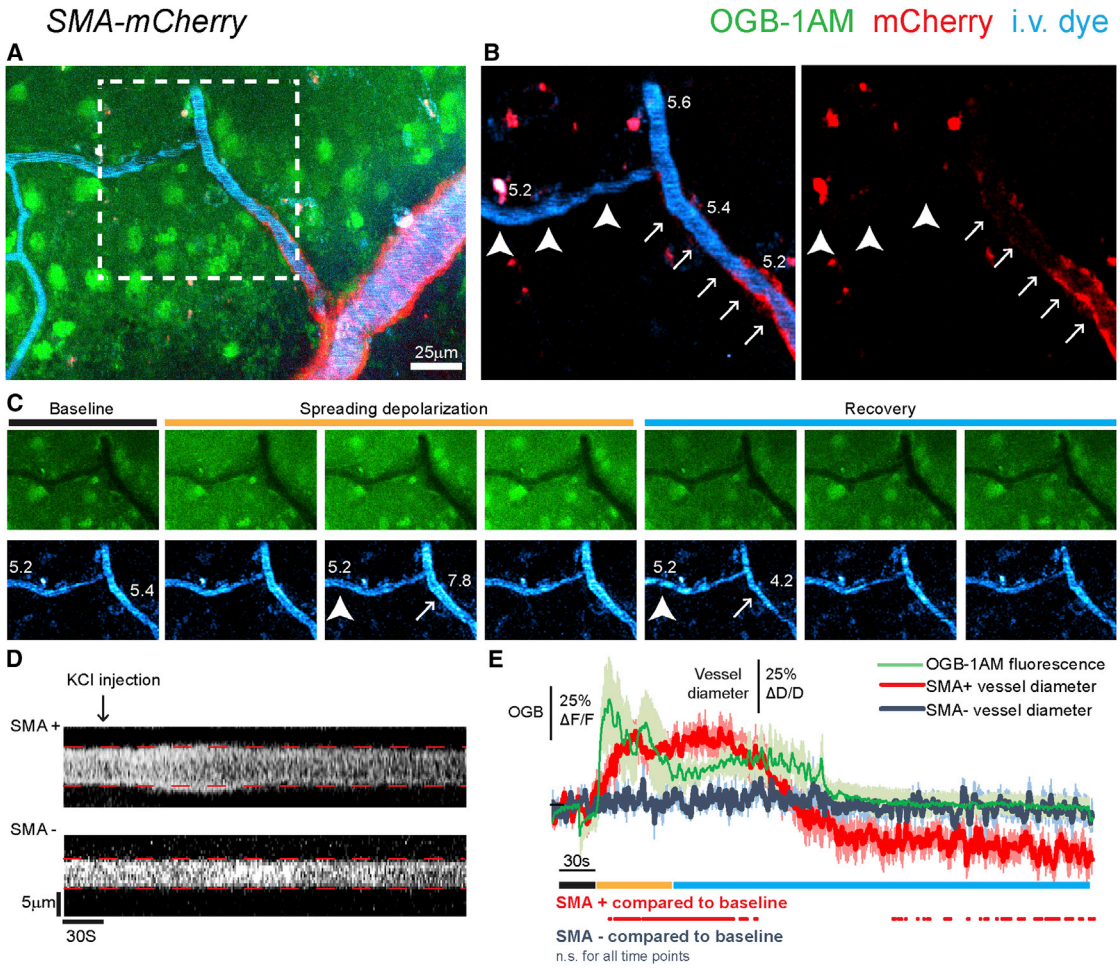

Figure 7. Cortical Spreading Depolarization Induces Vasomotion of Smooth Muscle but Not Pericyte-Covered Microvessels

(A) In vivo image captured from the cortex of an *SMA-mCherry* (red) transgenic mouse with neurons and astrocytes labeled with the Oregon Green Bapta-1AM (OGB-1AM) calcium indicator (green) and vessels labeled via intravascular dye (blue).

(B) Region depicted in (A) of the transition from precapillary SMA-covered vessel (arrows) to capillary pericyte-covered vessel (arrowheads); numbers indicate baseline vessel diameters.

(C) Time sequence showing the OGB-1AM fluorescence intensity and vessels at baseline, during KCl-induced spreading depolarization, and during the recovery period; numbers indicate vessel diameters.

(D) Line-scan time series images showing KCl-induced change in vessel diameter in an SMA+ vessel, but not in the downstream SMA– vessel.

(E) Quantification of the neuronal and vascular responses to spreading depolarization (gold bar) with the average neural OGB-1AM fluorescence signal (green), the average change in diameter of precapillary vessels with a smooth muscle layer (SMA+, red), and capillaries lacking a smooth muscle layer (SMA−, blue). Traces show mean values ± SEM, n = 10 SMA+ vessels, and 10 SMA− vessels from 3 mice. Asterisk indicates significance compared to baseline determined by a 99% confidence interval.

strongly suggest that in the awake mouse cortex, functional hyperemia is mediated by calcium-dependent arteriolar SMC contractility rather than direct capillary pericyte contractility.

Vasomotor Responses during Cortical Spreading Depolarization

Cortical spreading depolarization (CSD) occurs under numerous pathological situations and results in altered CBF (Leao, 1944; Somjen, 2001). To determine the precise location within the vascular tree of CSD-induced vasomotor responses, we loaded neural cells with the calcium-sensitive dye Oregon Green Bapta 1AM (OGB) in *SMA-mCherry* transgenic mice that had been intravenously injected with a fluorescent dye to visualize the vessel lumen (Figures 7A and 7B).

To induce CSD, we performed a single microinjection of 0.5 M potassium chloride (KCl) 1–2 mm from the imaging site. As predicted, these injections resulted in prolonged increases in OGB fluorescence intensity in neurons and astrocytes consistent with the time course of CSD (Somjen, 2001) (Figures 7C–7E). We detected significant diameter changes during CSD that occurred exclusively in vessels with a smooth muscle layer (~25% increase at peak dilation, ~10% decrease at peak constriction, significance determined by a 99% confidence interval, n = 10 vessels from 3 mice), but not in capillaries with

pericytes that lack SMA (n = 10 vessels from 3 mice) (Figures 7C–7E). Therefore, consistent with the optogenetic and sensory-evoked experiments above, modulation of blood flow during CSD is mediated by smooth muscle-covered vessels and not by capillary pericytes.

Transient MCA Occlusion Induces Focal SMC Constriction and Reperfusion Deficits

Finally, we tested if cerebral ischemia could induce focal constrictions in microvessels that could prevent re-establishment of blood flow. We implemented a transient (90 min) filament occlusion of the middle cerebral artery (tMCAO) (see Experimental Procedures), and we performed in vivo imaging of cerebral MCA branches before, during, after and 4 hr after reperfusion (Figures 8A, S6A, and S6B). Consistent with our previous experiments, we focused our analysis on the transition points between the last SMC on precapillary arterioles and pericytes on capillaries using *SMA-mCherry* and *NG2creER:mT/mG* transgenic mice.

In order to sample a large region during and after tMCAO, high-resolution tiled images covering the entire cranial window were acquired (Figure S6). Confirmation of vessel occlusion during tMCAO was determined by the presence of sluggish and turbulent CBF and corresponding hypoxia-induced vessel dilation evident in 20–30 μm diameter pial arterioles (Figure S6C). Precapillary arteriolar-to-capillary transitions were analyzed in these vessels by noting and measuring changes in vessel perfusion and diameter. We observed multiple outcomes both during and after the tMCAO, particularly at the last SMC. These terminal SMCs often displayed focal constrictions that were transient and observed only during MCAO or induced during MCAO and maintained after reperfusion (Figures 8B–8E, S7, and S8A). These focal SMC constrictions resulted in RBC perfusion block to downstream capillaries which either maintained some plasma flow (Figures 8E and S7; Movie S4, Movie S5, and Movie S6) or displayed complete vessel occlusion (Figures 8B–8D and S7). RBC perfusion block was observed in 48 out of 59 SMC-to-pericyte transitions with 21 and 27 of those displaying reversible or maintained focal SMC constrictions, respectively (Figures 8F and 8G). Focal constrictions in capillaries were not observed (Figures 8, S7, and S8) even at the location of pericyte cell bodies, 4 and 24 hr after tMCAO, as previously reported (Hall et al., 2014) (Figure S8). Measurement of vessel diameter in RBC perfusion blocked SMC-to-pericyte transitions (see Figure 8F for measurement location diagram) revealed a significant average decrease in vessel diameter at terminal SMCs, but not in downstream same-branch or second-branch pericyte-covered capillaries (Figure 8H) (n = 51 terminal SMC-covered precapillary arterioles, 51 same-branch capillaries, and 27 second-branch capillaries from 5 mice; significance determined by unpaired two-tailed t test). Further characterization of all SMC to pericyte transitions revealed a variety of perfusion and vessel change outcomes during and after tMCAO (Figure 8I). These outcomes were characterized as maintained RBC perfusion (Figure S10E), only plasma perfusion (Figures 8 and S7), complete block with thrombus (Figures 8 and S7), or vessel collapse/no intravascular dye (Figures S7B and S7E) (defined as collapse or no i.v. dye labeling spanning greater than 20 μm vessel length).

Overall, these data suggest that during cerebral ischemia and reperfusion, SMCs display focal constrictions that are transient or prolonged. In combination with numerous other cellular processes taking place during cerebral ischemia, these SMC constrictions appear to play a significant role as an early mechanism that prevents tissue reflow, leading to potentially irreversible microvascular occlusion.

DISCUSSION

We have precisely identified and functionally characterized in vivo the contractile perivascular mural cells that control neurovascular coupling and microregional CBF. Our results demonstrate that CBF regulation takes place exclusively at microvessels covered by SMCs that have a distinct circumferential morphology and express SMA (Figure S9). Several lines of evidence demonstrate that capillary pericytes, which do not express SMA and have a noncircumferential, longitudinal morphology spanning long distances, do not have the capacity for direct regulation of blood flow. First, in vivo spontaneous vasomotion in awake mice occurs in vessels covered by SMCs, regardless of their diameter or branch order, but does not occur in pericyte-covered vessels. Second, spontaneous calcium fluctuations in SMCs correlate with vessel diameter changes, while calcium fluctuations in pericytes do not induce changes in capillary diameter. Third, single-cell in vivo optogenetic activation of SMCs causes vessel constriction and flow reductions, while identical activation of pericytes causes no capillary changes. Fourth, sensory stimulation evokes a rapid and robust dilation of SMC-covered vessels, but only a slow and nearly undetectable dilation of pericyte-covered capillaries which is likely to be passive. Fifth, CSD induces active vasomotion in SMC-covered vessels, but not in pericyte-covered capillaries. These multiple lines of independent in vivo evidence demonstrate unambiguously that capillary pericytes are not contractile and thus cannot directly regulate CBF.

While the capillary network comprises the majority of the brain vascular system, our data demonstrate that direct regulation of blood flow occurs at the level of arteries, arterioles, and precapillaries. Our findings describing mural cell contractility and control of CBF by arterioles greater than 10 μm in diameter are consistent with a number of previous studies using tissue explant preparations (Borysova et al., 2013; Kornfield and Newman, 2014) and in vivo brain vessel imaging (Devor et al., 2007; Drew et al., 2011; Fernández-Klett et al., 2010; Iadecola et al., 1997; Kornfield and Newman, 2014; Vanzetta et al., 2005). Importantly, however, we have for the first time precisely established a direct relationship between microvascular mural cell molecular identity, single-cell morphology, and cellular function at each level of the cerebral vascular tree in vivo. We unambiguously demonstrate that in vessels smaller than 10 μm in diameter, at the transition between SMC and pericyte-covered regions, there is great heterogeneity of contractile properties.

It is critical to note that vascular diameter and vessel branch order are not reliable determinants of contractile capacity as microvessels smaller than 10 μm in diameter, with branch orders ranging from first to fourth, are enveloped by mural cells with heterogeneous SMA expression and contractile capacity. Previous

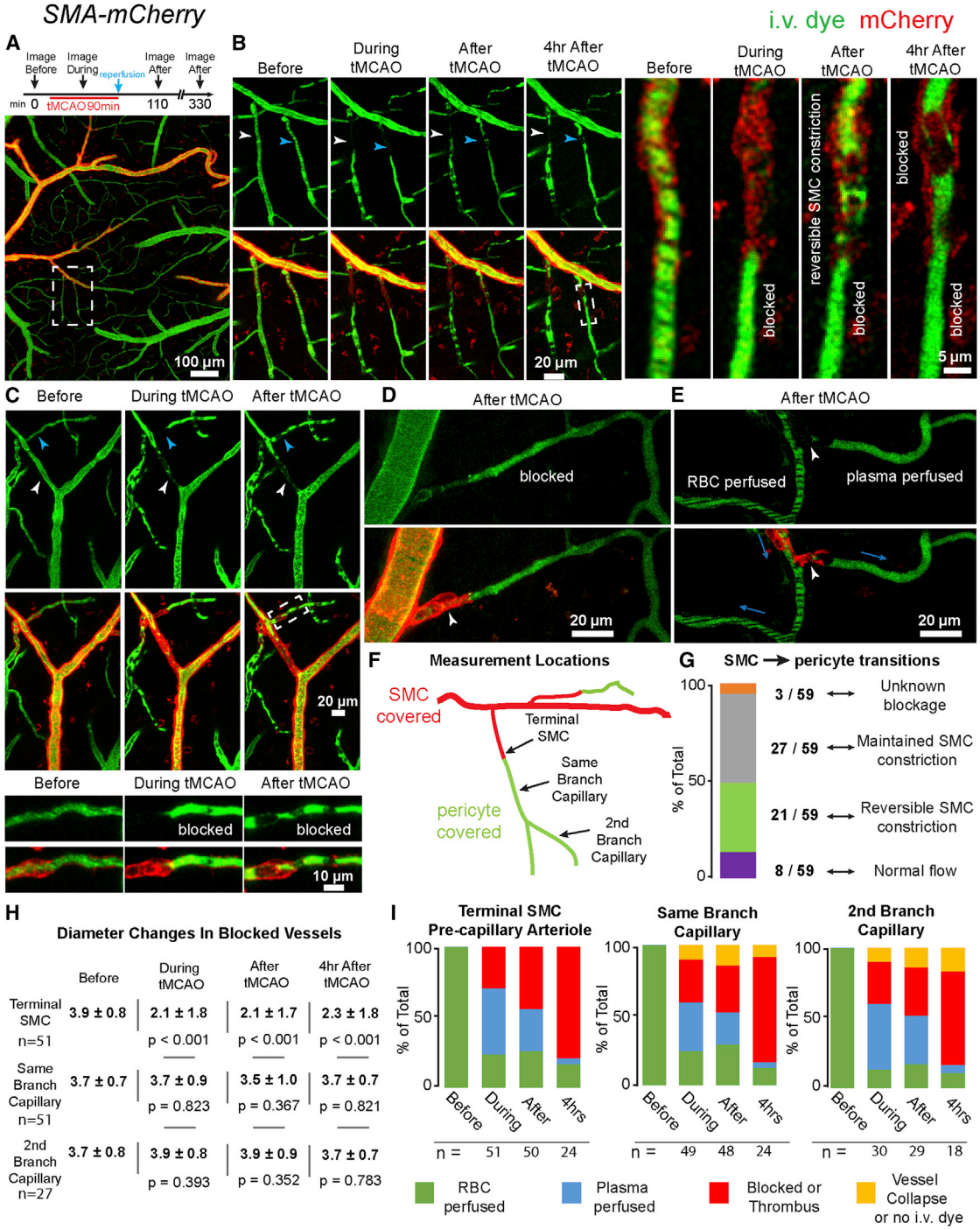

Figure 8. Transient MCA Occlusion Induces Focal SMC Constriction and Reperfusion Deficits

(A) Timeline for experimental transient (90 min) middle cerebral artery occlusion (tMCAO) with in vivo imaging. In vivo image from an *SMA-mCherry* transgenic mouse (red) with intravascular dye (green) showing an example of a transition from SMC to pericyte-covered vessels depicted in (B).

(B and C) Repeated in vivo images captured before, during, after, and 4 hr after tMCAO showing prolonged (white arrowheads) or transient (blue arrowheads) SMC focal constrictions with maintained subsequent vessel blockage in downstream capillaries. Right-side panels in (B) are zoomed from boxed region.

(D and E) Example vessel perfusion outcomes (blocked, plasma perfused, or RBC perfused) after SMC focal constrictions (arrowheads) due to tMCAO.

(F) Diagram showing the measurement locations on the vascular tree at the transition points between SMCs and pericytes for quantification in (G)–(I).

(G) Vessel perfusion outcomes 4 hr after tMCAO for all SMC to pericyte transitions; n = 59 transitions from 5 mice.

(legend continued on next page)

studies have relied on vessel diameter, branch order, or both to distinguish between arterioles and terminal capillaries. This distinction cannot discriminate between SMA-expressing precapillary SMCs and SMA-deficient capillary pericytes, and likely contributes to seemingly contradictory conclusions from our study and others (Fernández-Klett et al., 2010; Hall et al., 2014). In addition to discrepancies from identifying terminal capillaries by their location and size, it should also be noted that all mural cells, including SMA-expressing SMCs, express the NG2 chondroitin sulfate proteoglycan and PDGFRβ (Armulik et al., 2011; Nakayama et al., 2013; Uemura et al., 2002). Therefore, NG2 and PDGFRβ expression cannot be used to unambiguously distinguish pericytes from SMCs. Thus far, the only reliable means to identify contractile vessels, particularly those with diameters less than 10 μm, is by SMA expression and the distinction between circumferential band-like SMC versus longitudinal pericyte morphologies.

The morphology of capillary pericytes provides some clues about their functional role. In stark contrast with the robust circumferential arrangement of SMCs, pericytes have thin processes that extend longitudinally for distances of up to ~300 μm, span multiple capillaries, and rarely wrap around vessels (Figure S1). This arrangement does not appear to be structurally suited for exerting radial forces capable of executing vessel diameter changes. The observation that capillaries can have even larger diameters than precapillary arterioles (Figures 2A and 4G) is highly suggestive of pericytes not even providing a baseline contractile tone to the vessel. In addition to these observations, the logic for altering vessel diameter at the capillary level as a mechanism for flow regulation is not clear. It is well documented that RBCs need to undergo cell deformation in order to move through 3–5 μm capillaries (Noguchi and Gompper, 2005; Pawlik et al., 1981; Skalak and Branemark, 1969). Thus, if contractility existed in capillaries, it is likely that even small changes in diameter would result in RBC perfusion block rather than a graded change in flow, posing a significant risk of focal microvascular thrombosis. We speculate that this phenomenon explains why small precapillary vessels with terminal SMCs are prone to irreversible distal microvascular occlusions after SMC constriction during cerebral ischemia.

Instead of a contractile role for pericytes, we speculate that the long, thin pericyte processes could provide a network for sensing, transmitting, or coordinating information between the neural and vascular compartments. Gap junction coupling between pericytes and endothelial and SMCs has been demonstrated (Borysova et al., 2013; Cuevas et al., 1984; Oku et al., 2001). Together with astrocytes (Simard et al., 2003), pericytes may play a role in coordinating neurovascular coupling (Itoh and Suzuki, 2012) through SMC contractility. Recent findings showing sensory-evoked dilation in first-order vessels prior to zero-order penetrating arterioles (Hall et al., 2014) could be explained if the signal to induce vasomotion is transmitted through local astrocytes and pericytes up the vascular tree, reaching SMC-covered precapillary arterioles prior to upstream arterioles. Intercellular communication between mural cells could also partly explain some of the variability we observed in our correlation experiments between SMC calcium and vasomotion. This variability is likely due to a number of complex interactions between proximal and distal SMCs and how upstream and downstream changes in diameter can alter blood flow and resistance, which could then independently alter vessel diameter in the absence of active vasomotion at the location of our SMC calcium measurements. However, even with these complex flow dynamics and cellular interactions, a highly significant anticorrelation was present between vasomotion and calcium fluctuations in arteriolar SMCs but was absent from capillary pericytes.

In neuropathological states, such as ischemia, irreversible pericyte constriction and death have been suggested to impair capillary reflow (Hall et al., 2014; Yemisci et al., 2009). Instead, we found that during early stages of ischemia and reperfusion after MCA occlusion, focal constrictions occur exclusively in vessels surrounded by SMCs (Figure S10). These constrictions were either transient or maintained and appeared to lead to downstream microvascular occlusion. We believe that the contradictory observations of vascular contractility in ischemia could stem from differences in experimental approaches (Vates et al., 2010) and from the belief that pericytes express SMA in vivo (Yemisci et al., 2009) and that SMCs are not located on brain vessels other than zero-order penetrating arterioles (Hall et al., 2014), which leads to misidentification of SMCs as pericytes.

"No reflow" after ischemia is likely a multifaceted, complex phenomenon (Figure S10). The variable SMC contractile behaviors and downstream flow outcomes in our data suggest that there are numerous multicellular processes occurring during both ischemia and reperfusion. SMC constrictions likely contribute to the process by temporarily slowing or blocking flow and thus initiating lumen thrombotic mechanisms and impairing clot washout. However, additional intrinsic or extrinsic mechanisms affecting the microvasculature, including capillary plugging by leukocytes and platelets (del Zoppo et al., 1991), luminal entrapment of thromboemboli by endothelial lamellipodia (Grutzendler et al., 2014; Lam et al., 2010), and interstitial swelling (Rezkalla and Kloner, 2002), are likely to significantly contribute to microvascular occlusion, vessel collapse, and impaired reperfusion.

Our anatomical data of the percentage of vessels covered by SMA-expressing SMCs support a model in which CBF is directly regulated by ~8% (by length) of all intraparenchymal cerebral microvessels. Given the distribution of penetrating and precapillary arterioles (Blinder et al., 2013) and considering that only those covered by SMA can regulate vessel diameter, we speculate that the resolution of CBF regulation is on the order of a 75–150 μm radius of tissue. Therefore, while the demand for

(H) Average vessel diameter measurements ± SD at each location along the vascular tree before, during, after, and 4 hr after tMCAO specifically in blocked, noncollapsed vessels; n is indicated in table from 5 mice; p values obtained from unpaired t test.
(I) Analysis of vessel perfusion during, after, and 4 hr after tMCAO at distinct locations along the vascular tree; n is indicated from 5 mice.
See also Figures S6–S8 and S10, and Movie S4, Movie S5, and Movie S6.

CBF changes may be detected at single capillaries, regulation of functional hyperemia likely does not occur at this level, but instead at SMC-covered precapillaries that feed relatively larger brain volumes. In addition to advancing our understanding of local tissue oxygenation, this observation has significant implications for techniques that use changes in CBF as a correlate for neural activity. Given the spatial regulation of CBF we observed, BOLD fMRI and optical imaging of intrinsic signals (Grinvald et al., 1986) may have a fundamental hypothetical limit in spatial resolution, independent of their technical limitations for signal detection.

In addition to understanding normal CBF regulation, our findings have important implications for neuropathology. SMC malfunction on the already-small proportion of vessels covered by SMCs could induce dramatic changes in neurovascular coupling and CBF regulation for the entire brain. For example, cerebral amyloid angiopathy, which occurs in Alzheimer's disease due to arteriolar accumulation of amyloid (Farkas and Luiten, 2001; Iadecola, 2004), could cause SMC malfunction on the small proportion of proximal vessels, with major consequences on CBF regulation for an entire volume that we estimate to have a radius of 75–150 μm. Likewise, the functional outcome after occlusion or loss of single microvessels during aging and a number of disease states (Armulik et al., 2011; Faraci, 2011; Harb et al., 2013; Iadecola, 2004) likely depends on whether or not these vessels are covered by SMCs or pericytes. Therefore, careful analysis of distinct mural cells on single vessels directly affected by pathology is necessary to fully understand cerebrovascular malfunction in multiple disease states.

In summary, our study demonstrates that under normal and pathological states, microvascular SMCs control CBF and neurovascular coupling. These cells are morphologically, molecularly, and functionally distinct from capillary pericytes, despite the fact that they can be found on vessels traditionally defined as capillaries, based on vessel diameter and/or branch order. Thus, true cerebral capillary pericytes are not contractile in vivo and do not independently regulate CBF but may have as-of-yet unidentified noncontractile CBF regulatory functions.

EXPERIMENTAL PROCEDURES

Animals

All animal experiments were approved by the Yale University Institutional Animal Care and Use Committee (IACUC). See also Supplemental Experimental Procedures. The following transgenic mice were used: *NG2cre* (Zhu et al., 2008) (Jackson Labs number 008533), *NG2creER* (Zhu et al., 2011) (Jackson Labs number 008538), floxed ChR2-YFP (Madisen et al., 2012) (Jackson Labs number 012569), *SMA-mCherry* (Armstrong et al., 2010); *SMAcreER* (Wendling et al., 2009), mT/mG (Muzumdar et al., 2007) (Jackson Labs number 007676), *Tie2-GFP* (Motoike et al., 2000) (Jackson Labs number 003658), *Z/EG* (Novak et al., 2000) (Jackson Labs number 003920), floxed GCaMP3 (Zariwala et al., 2012) (Jackson Labs number 014538), and *Confetti* (Snippert et al., 2010) (Jackson Labs number 013731). Male and female mice aged 4–16 weeks were used and all experiments were in awake, alert, head-fixed mice or mice anesthetized via intraperitoneal injection of 100 mg/kg ketamine and 10 mg/kg xylazine (k/x) by body weight as indicated.

Cranial Window Surgery and In Vivo Imaging

An acute cranial window preparation was used for all in vivo imaging experiments as described previously (Hill and Grutzendler, 2014; Schain et al., 2014). For two-photon imaging, a mode-locked MaiTai laser (Spectra Physics) was used on a two-photon microscope (Prairie Technologies) with a 20× water immersion objective (Zeiss 1.0 NA). In some cases a confocal (Leica SP5) with a 20× water immersion objective (Leica 1.0 NA) was used for optimal fluorophore excitation and emission separation and for activation of channelrhodopsin (see below).

Channelrhodopsin Activation

Texas Red dextran (70,000 mw, Life Technologies catalog number D-1864) or Cascade Blue dextran (10,000mw, Life Technologies catalog number D-1976) were injected intravenously to label blood plasma and were used to determine changes in vessel diameter and flow velocity. Analysis of single-cell morphology (in addition to *SMA-mCherry* expression) as described in Figures 1–4 was carried out from high-resolution confocal or two-photon z stacks of single mural cells expressing YFP fused to ChR2 that were acquired using light wavelengths which were not optimal for stimulation of ChR2 but sufficient for YFP excitation and detection (561 nm for confocal and 900 nm for two photon) in order to avoid any chance of ChR2 stimulation due to imaging alone. To activate ChR2, a laser line-scan or ROI-based local activation was used. We used a 473/488 nm confocal laser line-scan activation protocol for optimal excitation of ChR2. In order to avoid potential artifacts from out-of-focus light-activating upstream vessels and causing nonspecific changes in flow, we used two-photon laser stimulation (tuned to 800 nm) (Duan et al., 2014) to determine the effect of single-cell activation on blood flow. While both were effective at causing activation of ChR2, each method proved optimal for diameter and flow measurements, respectively.

Whisker Stimulation

We used the mouse whisker sensory system to test the effects of external sensory input on diameter of vessels with and without smooth muscle expression in the awake mouse somatosensory cortex (Figure 6). After cranial window surgeries, mice were allowed to recover from anesthesia before two-photon imaging and sensory stimulation. Dextran was injected intravenously to label blood vessels and was used to determine changes in vessel diameter described in data analysis. Whisker stimulation was done in awake head-fixed mice using a small tube attached to a picospritzer (set to 30 psi) positioned 1–2 cm from the contralateral vibrissae. Stimulation consisted of 100 ms air puffs at 5 Hz for 2 or 30 s as indicated.

Cortical Spreading Depolarization

To image vasomotor responses during CSD (Figure 7), 0.8 mM Oregon Green 488 BAPTA-1 AM (OGB) (Life Technologies catalog number O-6807) was pressure injected through a pulled glass micropipette. To induce CSD, 0.5 mM KCl was injected 1–2 mm away from the imaging location. Time-lapse imaging was performed before, during, and after the CSD induction in order to detect the change in calcium in neurons and astrocytes with OGB and correlate these changes with smooth muscle-labeled and nonlabeled vessel diameter changes with intravascular dye.

Ischemia-Reperfusion by Middle Cerebral Artery Filament Occlusion

Focal ischemia was induced by transient (90 min) middle cerebral artery occlusion (tMCAO) using an intraluminal filament technique. The carotid artery was exposed in the neck region, and a silicon rubber-coated 6-0 nylon monofilament with 2 mm tip (~230 μm diameter of the tip) was introduced into the common carotid artery and advanced 9 mm along the internal carotid artery (ICA) until occluding the origin of the MCA. After 90 min, the filament was withdrawn to establish reperfusion. Prior to MCAO, a cranial window was prepared, and imaging was performed using a two-photon or confocal microscope. Imaging was performed before, during, immediately after, and 4 hr after tMCAO. Vessel perfusion at each stage was determined via detection of RBC flux using i.v. dyes.

Tissue Processing, Imaging Data, and Statistical Analyses

Mice were anesthetized and perfused with 2% or 4% paraformaldehyde, and tissue was processed as outlined in Supplemental Experimental Procedures. Detailed descriptions for data analyses can also be found in Supplemental Experimental Procedures.

SUPPLEMENTAL INFORMATION

Supplemental Information includes ten figures, six movies, and Supplemental Experimental Procedures and can be found with this article at http://dx.doi.org/10.1016/j.neuron.2015.06.001.

AUTHOR CONTRIBUTIONS

R.A.H., L.T., and P.Y. designed and performed experiments and analyzed data. S.M. and S.G. performed experiments. R.A.H. and J.G. wrote the manuscript. J.G. designed and supervised the experiments.

ACKNOWLEDGMENTS

We thank K. Hirschi (Yale University) for sharing *SMA-mCherry* transgenic mice, D. Greif (Yale University) for sharing *SMAcreER* mice, A. Nishiyama (University of Connecticut) for sharing *NG2cre* mice, Z.J. Zhou (Yale University) for sharing ChR2-YFP and GCaMP3 mice, and M. Mesulam (Alzheimer Disease Center at Northwestern University) for providing postmortem human tissue. This work was supported by the following grants from the National Institutes of Health: R01-HL106815 and R01-NS089734 to J.G., and F32-NS090820 to R.A.H.

Received: January 14, 2015
Revised: April 24, 2015
Accepted: May 22, 2015
Published: June 25, 2015

REFERENCES

Armstrong, J.J., Larina, I.V., Dickinson, M.E., Zimmer, W.E., and Hirschi, K.K. (2010). Characterization of bacterial artificial chromosome transgenic mice expressing mCherry fluorescent protein substituted for the murine smooth muscle alpha-actin gene. Genesis *48*, 457–463.

Armulik, A., Genové, G., Mäe, M., Nisancioglu, M.H., Wallgard, E., Niaudet, C., He, L., Norlin, J., Lindblom, P., Strittmatter, K., et al. (2010). Pericytes regulate the blood-brain barrier. Nature *468*, 557–561.

Armulik, A., Genové, G., and Betsholtz, C. (2011). Pericytes: developmental, physiological, and pathological perspectives, problems, and promises. Dev. Cell *21*, 193–215.

Attwell, D., and Iadecola, C. (2002). The neural basis of functional brain imaging signals. Trends Neurosci. *25*, 621–625.

Bell, R.D., Winkler, E.A., Sagare, A.P., Singh, I., LaRue, B., Deane, R., and Zlokovic, B.V. (2010). Pericytes control key neurovascular functions and neuronal phenotype in the adult brain and during brain aging. Neuron *68*, 409–427.

Blinder, P., Tsai, P.S., Kaufhold, J.P., Knutsen, P.M., Suhl, H., and Kleinfeld, D. (2013). The cortical angiome: an interconnected vascular network with noncolumnar patterns of blood flow. Nat. Neurosci. *16*, 889–897.

Borysova, L., Wray, S., Eisner, D.A., and Burdyga, T. (2013). How calcium signals in myocytes and pericytes are integrated across in situ microvascular networks and control microvascular tone. Cell Calcium *54*, 163–174.

Brian, J.E., Faraci, F.M., and Feuerstein, G. (1998). Tumor necrosis factor-induced dilatation of cerebral arterioles editorial comment. Stroke *29*, 509–515.

Chaigneau, E., Oheim, M., Audinat, E., and Charpak, S. (2003). Two-photon imaging of capillary blood flow in olfactory bulb glomeruli. Proc. Natl. Acad. Sci. USA *100*, 13081–13086.

Cuevas, P., Gutierrez-Diaz, J.A., Reimers, D., Dujovny, M., Diaz, F.G., and Ausman, J.I. (1984). Pericyte endothelial gap junctions in human cerebral capillaries. Anat. Embryol. (Berl.) *170*, 155–159.

Daneman, R., Zhou, L., Kebede, A.A., and Barres, B.A. (2010). Pericytes are required for blood-brain barrier integrity during embryogenesis. Nature *468*, 562–566.

del Zoppo, G.J., Schmid-Schönbein, G.W., Mori, E., Copeland, B.R., and Chang, C.M. (1991). Polymorphonuclear leukocytes occlude capillaries following middle cerebral artery occlusion and reperfusion in baboons. Stroke *22*, 1276–1283.

Devor, A., Tian, P., Nishimura, N., Teng, I.C., Hillman, E.M.C., Narayanan, S.N., Ulbert, I., Boas, D.A., Kleinfeld, D., and Dale, A.M. (2007). Suppressed neuronal activity and concurrent arteriolar vasoconstriction may explain negative blood oxygenation level-dependent signal. J. Neurosci. *27*, 4452–4459.

Drew, P.J., Shih, A.Y., and Kleinfeld, D. (2011). Fluctuating and sensory-induced vasodynamics in rodent cortex extend arteriole capacity. Proc. Natl. Acad. Sci. USA *108*, 8473–8478.

Duan, X., Krishnaswamy, A., De la Huerta, I., and Sanes, J.R. (2014). Type II cadherins guide assembly of a direction-selective retinal circuit. Cell *158*, 793–807.

Faraci, F.M. (2011). Protecting against vascular disease in brain. Am. J. Physiol. Heart Circ. Physiol. *300*, H1566–H1582.

Farkas, E., and Luiten, P.G. (2001). Cerebral microvascular pathology in aging and Alzheimer's disease. Prog. Neurobiol. *64*, 575–611.

Fernández-Klett, F., Offenhauser, N., Dirnagl, U., Priller, J., and Lindauer, U. (2010). Pericytes in capillaries are contractile in vivo, but arterioles mediate functional hyperemia in the mouse brain. Proc. Natl. Acad. Sci. USA *107*, 22290–22295.

Grinvald, A., Lieke, E., Frostig, R.D., Gilbert, C.D., and Wiesel, T.N. (1986). Functional architecture of cortex revealed by optical imaging of intrinsic signals. Nature *324*, 361–364.

Grutzendler, J., Murikinati, S., Hiner, B., Ji, L., Lam, C.K., Yoo, T., Gupta, S., Hafler, B.P., Adelman, R.A., Yuan, P., and Rodriguez, G. (2014). Angiophagy prevents early embolus washout but recanalizes microvessels through embolus extravasation. Sci. Transl. Med. *6*, 226ra31.

Hall, C.N., Reynell, C., Gesslein, B., Hamilton, N.B., Mishra, A., Sutherland, B.A., O'Farrell, F.M., Buchan, A.M., Lauritzen, M., and Attwell, D. (2014). Capillary pericytes regulate cerebral blood flow in health and disease. Nature *508*, 55–60.

Hamel, E. (2006). Perivascular nerves and the regulation of cerebrovascular tone. J. Appl. Physiol. *100*, 1059–1064.

Hamilton, N.B., Attwell, D., and Hall, C.N. (2010). Pericyte-mediated regulation of capillary diameter: a component of neurovascular coupling in health and disease. Front. Neuroenergetics *2*, 1–14.

Harb, R., Whiteus, C., Freitas, C., and Grutzendler, J. (2013). In vivo imaging of cerebral microvascular plasticity from birth to death. J. Cereb. Blood Flow Metab. *33*, 146–156.

Haydon, P.G., and Carmignoto, G. (2006). Astrocyte control of synaptic transmission and neurovascular coupling. Physiol. Rev. *86*, 1009–1031.

Hill, R.A., and Grutzendler, J. (2014). In vivo imaging of oligodendrocytes with sulforhodamine 101. Nat. Methods *11*, 1081–1082.

Hill, R.A., Patel, K.D., Goncalves, C.M., Grutzendler, J., and Nishiyama, A. (2014). Modulation of oligodendrocyte generation during a critical temporal window after NG2 cell division. Nat. Neurosci. *17*, 1518–1527.

Iadecola, C. (2004). Neurovascular regulation in the normal brain and in Alzheimer's disease. Nat. Rev. Neurosci. *5*, 347–360.

Iadecola, C., and Nedergaard, M. (2007). Glial regulation of the cerebral microvasculature. Nat. Neurosci. *10*, 1369–1376.

Iadecola, C., Yang, G., Ebner, T.J., and Chen, G. (1997). Local and propagated vascular responses evoked by focal synaptic activity in cerebellar cortex. J. Neurophysiol. *78*, 651–659.

Itoh, Y., and Suzuki, N. (2012). Control of brain capillary blood flow. J. Cereb. Blood Flow Metab. *32*, 1167–1176.

Kety, S.S., and Schmidt, C.F. (1948). The effects of altered arterial tensions of carbon dioxide and oxygen on cerebral blood flow and cerebral oxygen consumption of normal young men. J. Clin. Invest. *27*, 484–492.

Kornfield, T.E., and Newman, E.A. (2014). Regulation of blood flow in the retinal trilaminar vascular network. J. Neurosci. *34*, 11504–11513.

Krueger, M., and Bechmann, I. (2010). CNS pericytes: concepts, misconceptions, and a way out. Glia *58*, 1–10.

Lam, C.K., Yoo, T., Hiner, B., Liu, Z., and Grutzendler, J. (2010). Embolus extravasation is an alternative mechanism for cerebral microvascular recanalization. Nature *465*, 478–482.

Leao, A.A.P. (1944). Spreading depression of activity in the cerebral cortex. J. Neurophysiol. *7*, 359–390.

Logothetis, N.K., and Wandell, B.A. (2004). Interpreting the BOLD signal. Annu. Rev. Physiol. *66*, 735–769.

Logothetis, N.K., Pauls, J., Augath, M., Trinath, T., and Oeltermann, A. (2001). Neurophysiological investigation of the basis of the fMRI signal. Nature *412*, 150–157.

Madisen, L., Mao, T., Koch, H., Zhuo, J.M., Berenyi, A., Fujisawa, S., Hsu, Y.-W.A., Garcia, A.J., 3rd, Gu, X., Zanella, S., et al. (2012). A toolbox of Cre-dependent optogenetic transgenic mice for light-induced activation and silencing. Nat. Neurosci. *15*, 793–802.

Motoike, T., Loughna, S., Perens, E., Roman, B.L., Liao, W., Chau, T.C., Richardson, C.D., Kawate, T., Kuno, J., Weinstein, B.M., et al. (2000). Universal GFP reporter for the study of vascular development. Genesis *28*, 75–81.

Muzumdar, M.D., Tasic, B., Miyamichi, K., Li, L., and Luo, L. (2007). A global double-fluorescent Cre reporter mouse. Genesis *45*, 593–605.

Nakayama, A., Nakayama, M., Turner, C.J., Höing, S., Lepore, J.J., and Adams, R.H. (2013). Ephrin-B2 controls PDGFRβ internalization and signaling. Genes Dev. *27*, 2576–2589.

Nishiyama, A., Suzuki, R., and Zhu, X. (2014). NG2 cells (polydendrocytes) in brain physiology and repair. Front. Neurosci. *8*, 133.

Noguchi, H., and Gompper, G. (2005). Shape transitions of fluid vesicles and red blood cells in capillary flows. Proc. Natl. Acad. Sci. USA *102*, 14159–14164.

Novak, A., Guo, C., Yang, W., Nagy, A., and Lobe, C.G. (2000). *Z/EG*, a double reporter mouse line that expresses enhanced green fluorescent protein upon Cre-mediated excision. Genesis *28*, 147–155.

O'Farrell, F.M., and Attwell, D. (2014). A role for pericytes in coronary no-reflow. Nat. Rev. Cardiol. *11*, 427–432.

Ogawa, S., Lee, T.M., Kay, A.R., and Tank, D.W. (1990). Brain magnetic resonance imaging with contrast dependent on blood oxygenation. Proc. Natl. Acad. Sci. USA *87*, 9868–9872.

Oku, H., Kodama, T., Sakagami, K., and Puro, D.G. (2001). Diabetes-induced disruption of gap junction pathways within the retinal microvasculature. Invest. Ophthalmol. Vis. Sci. *42*, 1915–1920.

Pawlik, G., Rackl, A., and Bing, R.J. (1981). Quantitative capillary topography and blood flow in the cerebral cortex of cats: an in vivo microscopic study. Brain Res. *208*, 35–58.

Peppiatt, C.M., Howarth, C., Mobbs, P., and Attwell, D. (2006). Bidirectional control of CNS capillary diameter by pericytes. Nature *443*, 700–704.

Puro, D.G. (2007). Physiology and pathobiology of the pericyte-containing retinal microvasculature: new developments. Microcirculation *14*, 1–10.

Raichle, M.E., and Mintun, M.A. (2006). Brain work and brain imaging. Annu. Rev. Neurosci. *29*, 449–476.

Rezkalla, S.H., and Kloner, R.A. (2002). No-reflow phenomenon. Circulation *105*, 656–662.

Rouget, C. (1874). Note on the development of the contractile walls of blood vessels. C. R. Acad. Sci. *79*, 559–562.

Roy, C.S., and Sherrington, C.S. (1890). On the regulation of the blood-supply of the brain. J. Physiol. *11*, 85–158.17.

Sagare, A.P., Bell, R.D., Zhao, Z., Ma, Q., Winkler, E.A., Ramanathan, A., and Zlokovic, B.V. (2013). Pericyte loss influences Alzheimer-like neurodegeneration in mice. Nat. Commun. *4*, 2932.

Sakagami, K., Wu, D.M., and Puro, D.G. (1999). Physiology of rat retinal pericytes: modulation of ion channel activity by serum-derived molecules. J. Physiol. *521*, 637–650.

Schain, A.J., Hill, R.A., and Grutzendler, J. (2014). Label-free in vivo imaging of myelinated axons in health and disease with spectral confocal reflectance microscopy. Nat. Med. *20*, 443–449.

Shen, Z., Lu, Z., Chhatbar, P.Y., O'Herron, P., and Kara, P. (2012). An artery-specific fluorescent dye for studying neurovascular coupling. Nat. Methods *9*, 273–276.

Simard, M., Arcuino, G., Takano, T., Liu, Q.S., and Nedergaard, M. (2003). Signaling at the gliovascular interface. J. Neurosci. *23*, 9254–9262.

Skalak, R., and Branemark, P.I. (1969). Deformation of red blood cells in capillaries. Science *164*, 717–719.

Snippert, H.J., van der Flier, L.G., Sato, T., van Es, J.H., van den Born, M., Kroon-Veenboer, C., Barker, N., Klein, A.M., van Rheenen, J., Simons, B.D., and Clevers, H. (2010). Intestinal crypt homeostasis results from neutral competition between symmetrically dividing Lgr5 stem cells. Cell *143*, 134–144.

Somjen, G.G. (2001). Mechanisms of spreading depression and hypoxic spreading depression-like depolarization. Physiol. Rev. *81*, 1065–1096.

Uemura, A., Ogawa, M., Hirashima, M., Fujiwara, T., Koyama, S., Takagi, H., Honda, Y., Wiegand, S.J., Yancopoulos, G.D., and Nishikawa, S. (2002). Recombinant angiopoietin-1 restores higher-order architecture of growing blood vessels in mice in the absence of mural cells. J. Clin. Invest. *110*, 1619–1628.

Vanzetta, I., Hildesheim, R., and Grinvald, A. (2005). Compartment-resolved imaging of activity-dependent dynamics of cortical blood volume and oximetry. J. Neurosci. *25*, 2233–2244.

Vates, G.E., Takano, T., Zlokovic, B., and Nedergaard, M. (2010). Pericyte constriction after stroke: the jury is still out. Nat. Med. *16*, 959, author reply, 960.

Wendling, O., Bornert, J.-M., Chambon, P., and Metzger, D. (2009). Efficient temporally-controlled targeted mutagenesis in smooth muscle cells of the adult mouse. Genesis *47*, 14–18.

Winkler, E.A., Bell, R.D., and Zlokovic, B.V. (2011). Central nervous system pericytes in health and disease. Nat. Neurosci. *14*, 1398–1405.

Winkler, E.A., Sagare, A.P., and Zlokovic, B.V. (2014). The pericyte: a forgotten cell type with important implications for Alzheimer's disease? Brain Pathol. *24*, 371–386.

Yemisci, M., Gursoy-Ozdemir, Y., Vural, A., Can, A., Topalkara, K., and Dalkara, T. (2009). Pericyte contraction induced by oxidative-nitrative stress impairs capillary reflow despite successful opening of an occluded cerebral artery. Nat. Med. *15*, 1031–1037.

Zariwala, H.A., Borghuis, B.G., Hoogland, T.M., Madisen, L., Tian, L., De Zeeuw, C.I., Zeng, H., Looger, L.L., Svoboda, K., and Chen, T.-W. (2012). A Cre-dependent GCaMP3 reporter mouse for neuronal imaging in vivo. J. Neurosci. *32*, 3131–3141.

Zhu, X., Bergles, D.E., and Nishiyama, A. (2008). NG2 cells generate both oligodendrocytes and gray matter astrocytes. Development *135*, 145–157.

Zhu, X., Hill, R.A., Dietrich, D., Komitova, M., Suzuki, R., and Nishiyama, A. (2011). Age-dependent fate and lineage restriction of single NG2 cells. Development *138*, 745–753.